

# Effect of Crystal Orientation on Nano-Cutting of Single Crystal $\gamma$ -TiAl Alloy

Li Junye, Xie Hongcai, Zhao Weihong, Zhang Xinming, Wang Fei, Shi Guangfeng

Ministry of Education Key Laboratory for Cross-Scale Micro and Nano Manufacturing, Changchun University of Science and Technology, Changchun 130022, China

**Abstract:** In order to study the effect of crystal orientation on the nano-cutting process of single crystal  $\gamma$ -TiAl alloy, molecular dynamic numerical methods were used to analyze and discuss the cutting force, cutting temperature, material removal and lattice structure changes of different cutting crystal directions, revealing different mechanism of crystal orientation on nano-cutting quality of single crystal  $\gamma$ -TiAl alloy. The results show that during the nano-cutting process, the cutting force, cutting temperature, material removal and lattice structure change with the change of crystal surface and crystal direction. When the (010) crystal plane is selected as the cutting plane, the cutting force is smaller, the generated cutting heat is less, the surface processing quality of the  $\gamma$ -TiAl alloy is better, and the lattice structure changes less. The workpiece in the direction of (010)[100] cutting crystals produces less cutting heat and is easier to cut with the least transformation of lattice structure and the best surface processing quality of the  $\gamma$ -TiAl alloy.

**Key words:** crystal orientation; nano-cutting; single crystal  $\gamma$ -TiAl alloy; material removal; molecular dynamics

As a highly efficient and precise processing and manufacturing method, nano-cutting has extremely important applications in the frontier science and technology fields, such as medical treatment, precision instrument and aerospace. Therefore, in order to deeply understand the nano-cutting mechanism, the microstructure of the material is used as the entry point. However, since the traditional cutting experiments can only observe the macroscopic phenomena, and the nano-cutting on material surface can only reach nanoscale or angstrom level, it is difficult to observe the complex microstructure changes of workpiece during the cutting process<sup>[1]</sup>. Molecular dynamics is a calculation method of material behavior based on the atomic scale. It is a powerful tool to overcome this difficulty. It can effectively describe the microstructural changes during nano-cutting<sup>[2,3]</sup>, and quantitatively characterize the cutting force<sup>[4]</sup>, cutting temperature<sup>[5,6]</sup> and other physical quanti-

ties, revealing the nano-cutting mechanism of various materials, such as single crystal copper<sup>[7,8]</sup> and single crystal aluminum<sup>[9]</sup>. Therefore, many researchers have studied the anisotropy of single crystal materials by molecular dynamics simulation.

Sharma et al<sup>[10]</sup> studied the anisotropy of single-crystal copper nano-cutting through molecular dynamics, and found that the surface quality was the highest and the material removal was the largest when it is cut along the (001)[110] crystal direction. Zhu and Fang<sup>[11]</sup> used molecular dynamics to conduct nanoscale processing on different planes of single-crystal copper, and found that the minimum material removal depth is related to crystal orientation. Lin and Shiu<sup>[12]</sup> used molecular dynamics to study the process of diamond nanocrystalline copper cutting, discussed the effect of crystal orientation on cutting force and surface morphology, and found that the appropriate rectangular

Received date: March 15, 2020

Foundation item: National Natural Science Foundation of China (51206011, U1937201); Science and Technology Development Program of Jilin Province (20200301040RQ); Project of Education Department of Jilin Province (JKH20190541KJ); Science and Technology Program of Changchun City (18DY017)  
Corresponding author: Zhang Xinming, Professor, Changchun University of Science and Technology, Changchun 130022, P. R. China, E-mail: fstving@163.com

Copyright © 2021, Northwest Institute for Nonferrous Metal Research. Published by Science Press. All rights reserved.

groove is obtained by cutting groove on (101) surface with rectangular tool. Xu et al<sup>[13]</sup> studied the effect of crystal orientation on the formation of single crystal aluminum surface and found that the cutting surface quality is better when the surface is cut along the crystal direction (110)[001], (110)[110] and (111)[110]. Komanduri et al<sup>[14,15]</sup> conducted molecular dynamics simulation to study the orientation effect of nano-cutting single crystal aluminum. Alhafez and Urbassek<sup>[16]</sup> systematically studied the effects of different surface orientations and cutting directions on nanocrystalline iron.

The crystal structures of single crystal copper and single crystal aluminum are face centered cubic (fcc) structure. The single crystal  $\gamma$ -TiAl alloy structure studied in this research is similar, except that the titanium atoms at the four face centers are replaced by aluminum atoms. The face centered tetragonal (fct) structure<sup>[17-19]</sup> forms determining the anisotropy of single crystal  $\gamma$ -TiAl alloy. At present, the anisotropy of single crystal  $\gamma$ -TiAl alloy is barely reported in the literature. It is essential to study the nano-cutting characteristics of single crystal  $\gamma$ -TiAl alloy with different crystal orientations. In this study, a molecular dynamics simulation method was used to perform nano-cutting on single crystal  $\gamma$ -TiAl alloy workpieces with diamond tools along different crystal orientations to study the effect of crystal anisotropy on the nano-cutting process. Three crystal planes (100), (010) and (110) were selected as cutting planes. Two typical crystal directions of each selected crystal plane were taken as cutting directions. Cutting force, cutting temperature, material removal and lattice structure of different cutting crystals were analyzed in the downward nano-cutting process.

## 1 Model Establishment and Selection of Potential Function

### 1.1 Model establishment

The single crystal  $\gamma$ -TiAl alloy has an  $L1_0$  type fct crystal structure. As shown in Fig.1, the lattice constants  $a_0$  and  $b_0$  are the sides of the upper and lower sides of the cuboid, and  $c_0$  is the height of the cuboid ( $a_0=b_0=0.4001$  nm,  $c_0=0.4181$  nm). The established nano-cutting model is shown in Fig.2. A single crystal  $\gamma$ -TiAl alloy was selected as the cutting workpiece. The model size was  $10\text{ nm}\times 16\text{ nm}\times 8\text{ nm}$ , and the spherical diamond particles with a lattice constant of  $0.357$  nm were selected as cutting tools. The radius of tool is  $1.5$  nm, and the number of tool atoms is 2485. The workpiece model was divided into three regions: boundary layer, constant temperature layer, and Newton layer. The boundary layer fixed the workpiece, the constant temperature layer transferred heat and ensured the heat exchange of the system, and the Newton layer was the processing area. In order to reduce the size effect during nano-cutting, periodic boundary conditions were adopted along the  $z$ -direction.

After the whole model was built, the initial temperature was set as  $293\text{ K}$ , and the nose-hoover hot bath method was used to relax the system and made the system reach the equilibrium state. Since the hardness of diamond is much greater than that of  $\gamma$ -TiAl alloy, the diamond tool was set as a rigid body, and the cutting depth was set as  $1\text{ nm}$ . In order to improve the calculation efficiency, after the relaxation was completed, the cutting speed was set as  $200\text{ m/s}$ , and the tool moved along the  $y$  direction to perform the cutting action, and the cutting distance was  $12\text{ nm}$ .

Three planes (001), (010) and (110) were selected as cutting planes, and two typical crystal directions on each selected plane were regarded as cutting directions, namely (001)[0 $\bar{1}$ 0], (001)[1 $\bar{1}$ 0], (010)[001], (010)[100], (110)[001] and (110)[1 $\bar{1}$ 0]. The crystal planes and crystal orientations are shown in Fig.3.

When the cutting direction is (001)[0 $\bar{1}$ 0], there are 78 000 atoms in the workpieces of the  $\gamma$ -TiAl alloy. The  $x$ -axis,  $y$ -axis and  $z$ -axis are [100], [010] and [001], respectively. The lattice spacing is  $a=b=a_0=0.4001\text{ nm}$ ,  $c=1.045 a_0=0.4181\text{ nm}$ .

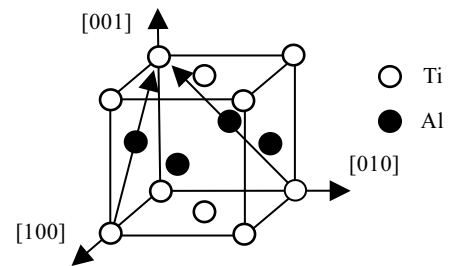


Fig.1 Lattice structure of  $\gamma$ -TiAl alloy

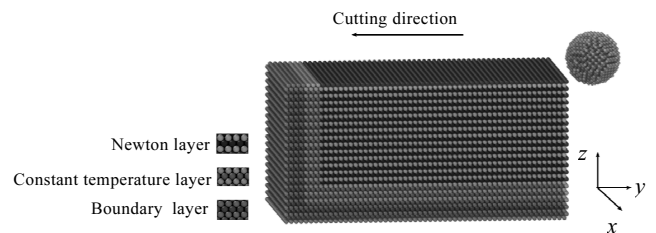


Fig.2 Molecular dynamics model of nano-cutting single crystal  $\gamma$ -TiAl alloy

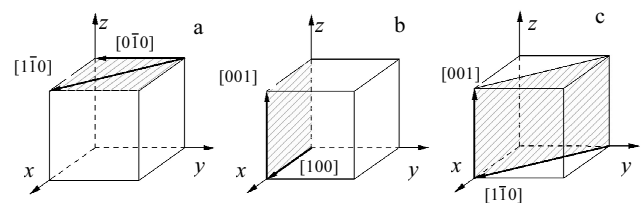


Fig.3 Schematic diagram of cutting direction on (001) (a), (010) (b), and (110) (c) crystal planes of single crystal  $\gamma$ -TiAl alloy

When the cutting direction is (001)[1 $\bar{1}$ 0], there are 78 945 atoms in the workpieces of the  $\gamma$ -TiAl alloy. The x-axis, y-axis and z-axis are [110], [ $\bar{1}$ 10] and [001], respectively. The lattice spacing is  $a=b=0.565827$  nm, and  $c=0.4181$  nm. When the cutting direction is (010)[001], there are 77 000 atoms in the workpieces of the  $\gamma$ -TiAl alloy. The x-axis, y-axis and z-axis are [100], [00 $\bar{1}$ ] and [010], respectively. The lattice spacing is  $a=c=0.4001$  nm, and  $b=0.4181$  nm. When the cutting direction is (010)[100], there are 76 800 atoms in the workpieces of the  $\gamma$ -TiAl alloy. The x-axis, y-axis and z-axis are [00 $\bar{1}$ ], [ $\bar{1}$ 00] and [010], respectively. The lattice spacing is  $a=0.4181$  nm, and  $b=c=0.4001$  nm. When the cutting direction is (110)[001], there are 77 956 atoms in the workpieces of the  $\gamma$ -TiAl alloy. The x-axis, y-axis and z-axis are [1 $\bar{1}$ 0], [00 $\bar{1}$ ] and [110], respectively. The lattice spacing is  $a=c=0.565827$  nm, and  $b=0.4181$  nm. When the cutting direction is (110)[1 $\bar{1}$ 0], there are 77 976 atoms in the workpieces of the  $\gamma$ -TiAl alloy. The x-axis, y-axis and z-axis are [00 $\bar{1}$ ], [ $\bar{1}$ 10] and [110], respectively. The lattice spacing is  $a=0.4181$  nm, and  $b=c=0.565827$  nm.

## 1.2 Selection of potential energy function

The interaction behavior between atoms is described by the potential function. In the process of numerical analysis of molecular dynamics, the interactions among Ti-Al, Ti-C and Al-C need to be considered because diamond abrasive grains are set as rigid bodies.

Embedded atomic method (EAM) potential can accurately describe the interaction between metal atoms. It is the most widely used interatomic potential in metals and alloys, which can effectively describe the interaction between metal atoms. In this study, the EAM potential was selected to describe the interaction potential between Ti-Al<sup>[20]</sup>, and the atomic energy is expressed as follows:

$$E = \sum_i F_i(\rho_i) + \frac{1}{2} \sum_{j \neq i} \Phi_{ij}(r_{ij}) \quad (1)$$

where  $F_i$  is the embedded energy function of the density of the atom  $i$ ,  $\rho_i$  is the electron cloud density of other atoms,  $\Phi_{ij}$  is the potential interaction function between the  $i$  atom and the  $j$  atom, and  $r_{ij}$  is the distance between the  $i$  atom and the  $j$  atom.

Morse potential function is a typical potential model based on the diatomic theory, which has a good approximation to the fine structure of atomic vibration. In this study, Morse potential was used to describe the interaction between Ti-C and Al-C<sup>[21]</sup>, and the expression is as follows:

$$E = D[e^{-2\alpha(r_{ij}-r)} - 2e^{-\alpha(r_{ij}-r)}] \quad (2)$$

where  $D$  is the binding energy,  $\alpha$  is the elastic modulus coefficient,  $r_{ij}$  is the distance between the  $i$  atom and the  $j$  atom, and  $r$  is the atomic spacing at equilibrium.

## 2 Analysis and Discussion

### 2.1 Influence of crystal orientation on cutting force

The removal of the workpiece material is due to the extrusion and shear action of the tool. So the cutting force of the tool atom on the workpiece atom can indirectly reflect the removal process of the workpiece material. In the process of nano-cutting, the tool atoms break the chemical bonds between the workpiece atoms, forcing the workpiece atoms to produce displacement, thus achieving the purpose of cutting. In order to study the ease of machining workpiece surface in different cutting directions, the change of cutting force along different cutting directions was analyzed. The change curves of main cutting force and normal cutting force along different cutting directions are shown in Fig.4.

Since the cutting direction of tool is the  $y$  direction, the cutting force  $F_y$  along the  $y$  direction is the main cutting force. Since the  $z$  direction is perpendicular to the cutting plane ( $xoy$ ), the cutting force  $F_z$  is a normal cutting force. It can be seen from Fig.4a and 4b that the nano-cutting process can be divided into an initial cutting stage and a stable cutting stage. With the increase of the cutting distance, both the main cutting force and the normal cutting force acting on the workpiece when it is cut along each crystal direction show a significant increase. This is the initial cutting stage. When the cutting distance reaches 3 nm, the tool completely cuts into the workpiece, and the cutting force no

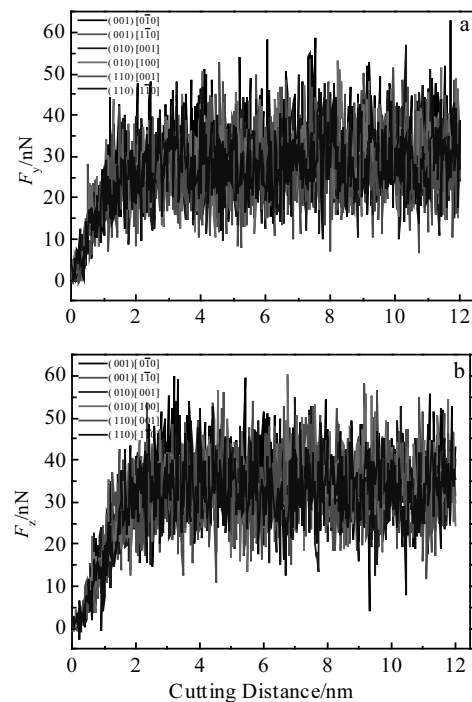


Fig.4 Curves of main cutting force  $F_y$  (a) and normal cutting force  $F_z$  (b) along different cutting directions

longer continues to increase, but fluctuates by a certain value. This is the stable cutting stage. The continuous fluctuation of the cutting force in the entire cutting process is mainly caused by the occurrence of lattice phase transformations, lattice reconstructions, the generation and combination of amorphous structures, and the evolution of microstructure defects in the workpiece.

It can be seen from Fig.4 that when the tool cuts along the  $(001)[0\bar{1}0]$  and  $(001)[1\bar{1}0]$  crystal directions, the main cutting force and the normal cutting force are larger, indicating that it is more difficult to cut. This is because the number of atoms accumulated in front of the tool is large, and a larger cutting force is required to achieve the purpose of material removal. Along the  $(110)[001]$  crystal direction, the smallest cutting force is required, indicating the easier direction to cut. When  $(001)$  and  $(010)$  crystal planes are selected as the cutting planes, the cutting force of the tool on the workpiece is relatively large. When the  $(110)$  crystal plane is selected as the cutting plane, the cutting force is relatively small, so it is easier to cut.

## 2.2 Influence of crystal orientation on cutting temperature

In the process of nano-cutting, the work done by the shear deformation of the chip and the friction between the tool and the workpiece is converted into cutting heat, which increases the temperature of the Newton layer of the workpiece, affecting the machining accuracy and surface quality of the workpiece. In order to study the change of cutting temperature along different cutting crystal directions, the temperature change in Newton layer of workpiece along different cutting crystal directions was analyzed. The temperature change curves of Newton layer of workpiece along different cutting crystal directions are shown in Fig.5.

As shown in Fig.5, with the increase of cutting distance, the temperature of the Newton layer in the workpiece increases rapidly. This is because the workpiece atoms are squeezed by the cutting tool, the chemical bonds between the workpiece atoms are destroyed, the workpiece atoms

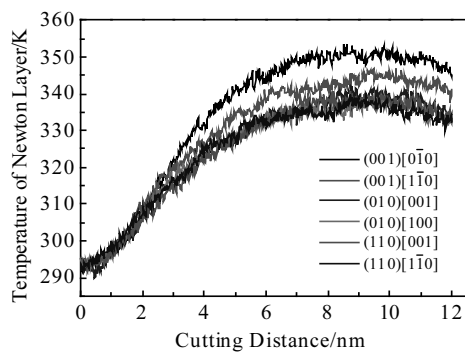


Fig.5 Curves of temperature change of Newton layer in workpiece along different cutting crystal orientations

produce displacement, the atomic kinetic energy increases, and a large amount of cutting heat is generated. When the cutting distance reaches 3 nm, the tool cuts into the workpiece completely, and the cutting process enters the stable cutting stage. The increasing trend of temperature in the Newton layer slows down, because the lattice reconstruction in the workpiece and the combination of amorphous atoms consume part of the energy. When the cutting distance is more than 10 nm, the temperature of the Newton layer decreases slowly. On the one hand, it is consumed by the lattice reconstruction and the combination of amorphous atoms. On the other hand, the cutting heat generated by the Newton layer can be quickly transferred to the constant temperature layer, accelerating the thermal balance of the workpiece.

When the cutting distance does not exceed 2 nm, the increasing trend of cutting temperature along each crystal direction is relatively close. With the increase of cutting distance, the generation of cutting heat gradually shows anisotropy. When the cutting direction is  $(001)[0\bar{1}0]$ , the temperature increase trend of Newton layer is the most obvious, and the cutting heat generated by the whole process is the greatest, followed by the cutting heat generated along the  $(001)[1\bar{1}0]$  crystal direction. This is because the work done by plastic deformation of the workpiece and the friction between the workpiece and the cutting tool is more, thereby, producing more cutting heat. In comparison, the cutting heat generated along the other four crystal directions is less and the difference is not large. When  $(001)$  crystal plane is selected as the cutting plane, the generated cutting heat is the greatest, and the temperature of Newton layer is the highest. When  $(010)$  and  $(110)$  crystal planes are selected as the cutting planes, the generated cutting heat is less, and the temperature of Newton layer is relatively low.

## 2.3 Influence of crystal orientation on material removal

In order to study the effect of different cutting crystal orientations on the removal of workpiece material, the surface morphology of different workpieces with different crystal orientations at a cutting distance of 10 nm was selected, as shown in Fig.6. Fig.6a~6f show the workpiece surface morphologies when the cutting direction is  $(001)[0\bar{1}0]$ ,  $(001)[1\bar{1}0]$ ,  $(010)[001]$ ,  $(010)[100]$ ,  $(110)[001]$  and  $(110)[1\bar{1}0]$ , respectively. The workpiece atoms are colored according to their heights along z-axis.

During the nano-cutting process, the atomic bond between the workpiece atoms breaks through the atomic pressure of the tool atoms, the workpiece atoms are displaced, a large number of atoms are stacked in front of the tool, and protrusions are generated on both sides of the groove produced by the cutting action of the tool, forming the flow measurement. As the cutting distance increases, more and more workpiece atoms accumulate in front of the

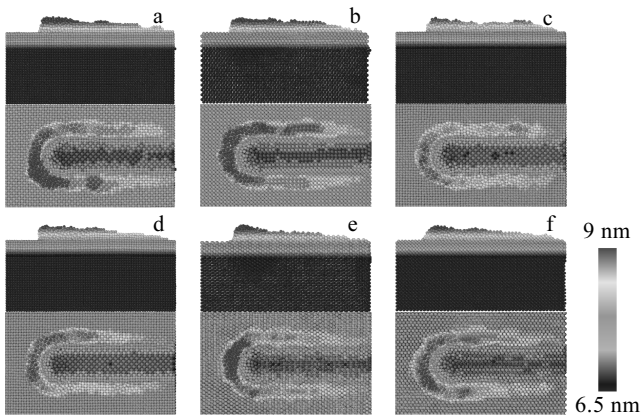


Fig.6 Surface morphologies of workpiece cut along (001)[010] (a), (001)[110] (b), (010)[001] (c), (010)[100] (d), (110)[001] (e), and (110)[110] (f) crystal orientations

tool. Some are removed as the chips, and some are retained on both sides of the groove as the flow measurement. It can be seen from Fig.6 that the crystal orientation has a great influence on the quality of the processed surface. The atomic stacking height caused by different cutting crystal directions is different. When the cutting directions are (001)[010] and (001)[110], the number of stacked atoms in front of the tool is more, i.e., the number of atoms removed by the material is the most. However, the number of removed atoms is smaller when the cutting directions are (010)[001] and (010)[100]. From the perspective of crystal plane selection, more atoms are removed when the crystal plane (001) is selected as the cutting plane, followed by the crystal plane (110), and the least material is removed when crystal plane (010) is the cutting plane.

In the process of nano-cutting, the existence of protrusions (side flow) on both sides of the workpiece groove is an important factor leading to the quality degradation of machining surface. Since the stacking height of the workpiece atoms on both sides of the groove is different, it is not convincing to judge the severity of the lateral flow phenomenon only by the lateral flow height. Therefore, when the cutting distance is 10 nm, the lateral flow height and the number of the lateral flow atoms along different cutting directions are counted, as shown in Fig.7 and Fig.8. It can be seen from Fig.7 and Fig.8 that the material accumulation of the workpiece on the side of the groove is the most obvious when cutting directions are (001)[010] and (001)[110]. While the material accumulation on the side of the groove is relatively small when the cutting directions are (010)[001] and (010)[100], and the machining quality is better (Fig.6). Although the sidestream height is the lowest when the cutting direction is (010)[001], the number of sidestream atoms is higher than that of the workpiece cut along (010)[100] crystal direction. This is due to the relatively

uniform stacking of workpiece atoms on both sides of the cutting groove along the cutting direction, as shown in Fig.6c and 6d. From the perspective of crystal plane selection, the material stacking height and the number of material atoms on the sides of grooves are the smallest when (010) crystal plane is selected as the cutting plane, followed by (110) crystal plane. While the amount of lateral stacking is the largest when (001) crystal plane is selected as the cutting plane. Although more atoms are removed from the (001) surface during cutting, the material accumulation on the sides of the grooves is the most obvious, which affects the quality of the processed surface.

#### 2.4 Effect of crystal orientation on lattice structure

In order to study the transformation of the atomic lattice structure of the workpiece along different cutting directions, the bond angle analysis method was used to identify the crystal structure of the workpiece along different cutting directions. The cutting layer structure of the workpiece along different cutting directions is shown in Fig.9. Fig.9a~9f show the cutting layer structure of the workpiece

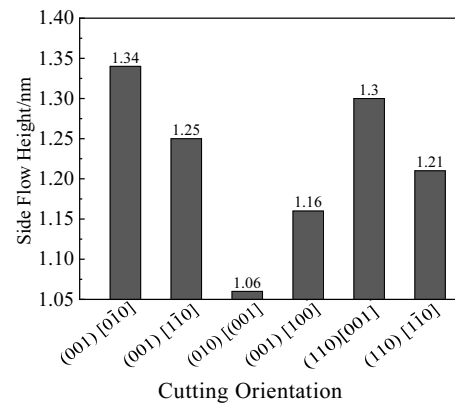


Fig.7 Comparison of lateral flow heights along different cutting crystal directions

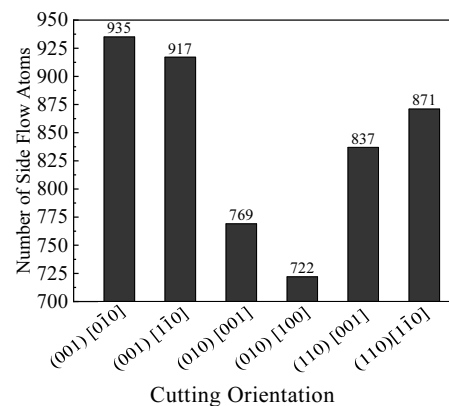


Fig.8 Comparison of the number of side flow atoms along different cutting crystal directions

when the cutting directions are  $(001)[0\bar{1}0]$ ,  $(001)[1\bar{1}0]$ ,  $(010)[001]$ ,  $(010)[100]$ ,  $(110)[001]$  and  $(110)[1\bar{1}0]$ , respectively. For the convenience of observation and analysis, the original fcc structure is hidden in the workpiece. White, red, blue, and yellow points represent other atoms, closely packed hexagonal (hcp) structure, body-centered cubic (bcc) structure and icosahedral structure (ico), respectively. And other atoms include surface atoms and defective face-centered cubic (dfcc) structure.

During the nano-cutting process, the workpiece is subjected to the extrusion and shearing action of the tool, and the lattice structure of the atom of the workpiece changes. Because the cutting forces of the workpiece atoms acting in different processing regions are different, the lattice structure of the workpiece cutting layer atoms is also different. As shown in Fig.9, due to the extrusion and shearing effect of the cutting tool, the original fcc lattice structure in workpieces with different cutting crystal orientations transforms into dfcc, hcp, bcc and ico structures. These lattice structures change with the increase of cutting distance and have different effects on the precision and quality of cutting. For quantitative analysis of lattice structure transformation along different cutting directions, the number of atoms of each lattice structure is small since only a few fcc structures transform into ico structures. So only the number of atoms of dfcc, hcp, bcc structures is shown in Fig.10. Fig.10a~10c show the number of atoms of dfcc, hcp, bcc structures, respectively, with the change of cutting distances along different cutting directions.

As shown in Fig.10, since more than 80% of the lattice structure of the  $\gamma$ -TiAl alloy is identified as fcc lattice structure, the number of atoms of dfcc structure is the

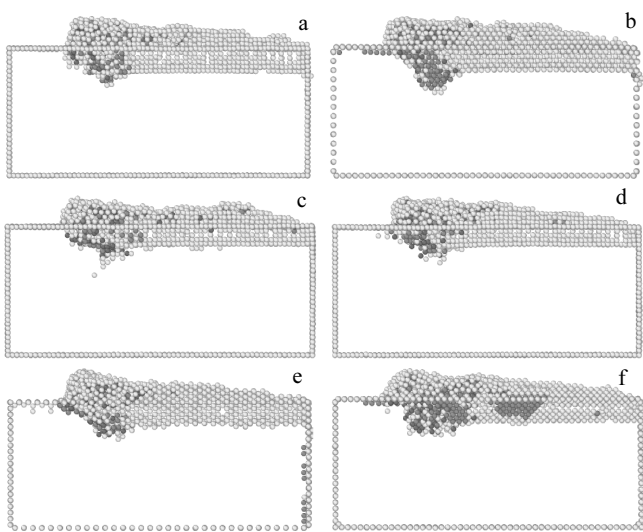


Fig.9 Structures of cutting layer of workpiece cut along  $(001)[0\bar{1}0]$ (a),  $(001)[1\bar{1}0]$ (b),  $(010)[001]$ (c),  $(010)[100]$ (d),  $(110)[001]$ (e), and  $(110)[1\bar{1}0]$ (f) crystal orientations

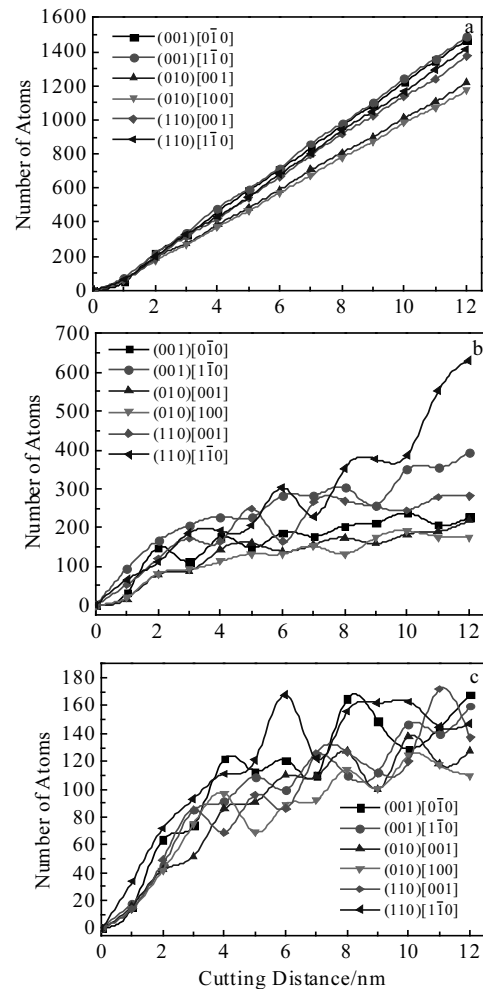


Fig.10 Number of atoms for transformation of dfcc (a), hcp (b), and bcc (c) lattice structures along different cutting directions

highest, followed by the number of atoms of hcp structure generated by the transformation of fcc lattice structure. The number of atoms of dfcc structure in different cutting directions is different. The number of atoms of dfcc structure generated along cutting directions  $(001)[0\bar{1}0]$  and  $(001)[1\bar{1}0]$  is the highest, while that generated along cutting directions  $(010)[001]$  and  $(010)[100]$  is the lowest. The number of atoms in dfcc structure generated by the transformation is related to the selected cutting plane. The number of dfcc structures at the same cutting plane generated by the transformation along different cutting directions is basically the same. The number of dfcc structures at  $(001)$  crystal plane is the largest, followed by the number of dfcc structures at  $(110)$  crystal plane, and the number of dfcc structures at  $(010)$  crystal plane is the smallest. The number of atoms of hcp structure is different along different cutting crystal directions. The number of atoms of hcp structure

along (110)[ $\bar{1}\bar{1}0$ ] direction is the greatest resulting from the transformation of fcc lattice structure. Then, the number of atoms of hcp structure generated along cutting directions (010)[001] and (010)[100] is the smallest. When the cutting distance exceeds 10 nm, the number of atoms of hcp structure generated by the transformation along (110)[ $\bar{1}\bar{1}0$ ] direction sharply increases. This is due to the nucleation, expansion and annihilation of the defects in the sub-surface of the workpiece. The atoms of original fcc structure transform into the atoms of hcp structure, which are stacked together in an abnormal stacking sequence. When [ $\bar{1}\bar{1}0$ ] crystal orientation is selected as the cutting direction, the number of atoms of hcp structure generated by the transformation is the greatest. When [001], [ $0\bar{1}0$ ], and [100] crystal orientations are selected as the cutting direction, the number of atoms of hcp structure generated by the transformation is small. This is because when the [ $\bar{1}\bar{1}0$ ] crystal orientation is selected as the cutting direction, the atomic arrangement of the workpiece is  $45^\circ$  from the tool. When the [001], [ $0\bar{1}0$ ], and [100] crystal orientations are selected as the cutting direction, the atomic arrangement of workpiece is  $0^\circ$  or  $180^\circ$  from the tool. The action form of the tool atom on the workpiece atom is different. In addition, the number of bcc structure produced by the fcc structure transformation is less affected by the cutting crystal orientation, and the number of atoms of bcc structure produced by different cutting crystal orientations is close. When the cutting direction is (010)[100], the number of bcc structures produced by the fcc structural transformation is small. When the cutting distance is 10 nm and the cutting direction is [ $\bar{1}\bar{1}0$ ], the number of atoms of bcc structure generated by transformation is the largest. When the cutting distance is 12 nm and the (001) cutting plane is selected, the number of atoms of bcc structure generated by transformation is the greatest, followed by the number of atoms of bcc structure when (110) crystal plane is selected. When the (010) cutting plane is selected, the number of atoms of bcc structure generated by transformation is the lowest. Therefore, the (010) crystal plane is more suitable to be the cutting plane, and the (010)[100] crystal orientation is the most suitable for cutting process for  $\gamma$ -TiAl alloy.

### 3 Conclusions

1) Compared with the results at (001) crystal plane, when the (010) and (110) crystal planes are selected as the cutting plane, the workpiece is easier to cut and less cutting heat is generated. The amount of material removed at (001) crystal plane is large, and the amount of atom accumulation on both sides of the groove is large. The amount of material removed at (010) and (110) crystal planes is small, and the side flow phenomenon is not obvious. When the (010) crystal plane is selected as the cutting plane, the number of atoms of dfcc and bcc structure produced by the fcc struc-

ture transformation is the smallest, and the number of atoms of two structures at (001) and (110) crystal planes are more. Therefore, the (010) crystal plane is more suitable to be the cutting plane.

2) When [ $\bar{1}\bar{1}0$ ] crystal direction is selected as the cutting direction, the number of atoms of hcp structure generated by fcc structure transformation is the largest. When [001], [ $0\bar{1}0$ ] and [100] crystal directions are selected as the cutting direction, the number of atoms of hcp structure generated by transformation is relatively small.

3) When the cutting direction is (010)[100], although the amount of material removed is small, the workpiece can be cut easily, the generated cutting heat is less, and the atoms of workpiece remain on both sides of the cutting groove transformed by the fcc structure. The generated dfcc, hcp and bcc structures have the least number of atoms, so the (010)[100] crystal orientation is the most suitable for cutting process for  $\gamma$ -TiAl alloy.

### References

- Xu F F, Fang F Z, Zhang X D. *Nanoscale Research Letters*[J], 2017, 12(1): 359
- Li J Y, Meng W Q, Dong K et al. *International Journal of Precision Engineering and Manufacturing*[J], 2018, 19(11): 1597
- Wang Q L, Zhang C F, Wu M P et al. *Nanoscale Research Letters*[J], 2019, 14(1): 239
- Gong Y D, Zhu Z X, Zhou Y G et al. *Science China Technological Sciences*[J], 2016, 59(12): 1837
- Zhu Y, Zhang Y C, Qi S H et al. *Rare Metal Materials and Engineering*[J], 2016, 45(4): 897 (in Chinese)
- Dai H F, Du H, Chen J B et al. *Proceedings of the Institution of Mechanical Engineers Part J: Journal of Engineering Tribology*[J], 2019, 233(8): 1208
- Wang Q L, Bai Q S, Chen J X et al. *Applied Surface Science*[J], 2015, 344: 38
- Li J, Fang Q H, Liu Y W et al. *Applied Surface Science*[J], 2014, 303: 331
- Alhafez I A, Gao Y, Urbassek H M. *Current Nanoscience*[J], 2017, 13(1): 40
- Sharma A, Datta D, Balasubramaniam R. *Computational Materials Science*[J], 2018, 153: 241
- Zhu P Z, Fang F F. *Computational Materials Science*[J], 2016, 118: 192
- Lin Y C, Shiu Y C. *The International Journal of Advanced Manufacturing Technology*[J], 2017, 89(9-12): 3207
- Xu F F, Fang F Z, Zhu Y Q et al. *Nanoscale Research Letters*[J], 2017, 12: 289
- Komanduri R, Chandrasekaran N, Raff L M. *Wear*[J], 2000, 242(1-2): 60
- Komanduri R, Chandrasekaran N, Raff L M. *Annals of the Cirp*[J], 1999, 48(1): 67

- 16 Alhafez I A, Urbassek H M. *Computational Materials Science*[J], 2018, 143: 286
- 17 Rui Z Y, Cao H, Luo D C et al. *Rare Metal Materials and Engineering*[J], 2017, 46(9): 2505 (in Chinese)
- 18 Feng R C, Qiao H Y, Zhu Z X et al. *Rare Metal Materials and Engineering*[J], 2019, 48(5): 1559 (in Chinese)
- 19 Cao H, Rui Z Y, Feng R C et al. *Rare Metal Materials and Engineering*[J], 2019, 48(4): 1102
- 20 Daw M S, Baskes M I. *Physical Review B*[J], 1984, 29(12): 6443
- 21 Girifalco L A, Weizer V G. *Physical Review*[J], 1959, 114(3): 687

## 晶体取向对单晶 $\gamma$ -TiAl 合金纳米切削的影响研究

李俊焯, 解鸿偲, 赵伟宏, 张心明, 王菲, 石广丰  
(长春理工大学 跨尺度微纳制造教育部重点实验室, 吉林 长春 130022)

**摘要:** 为了研究晶体取向对单晶  $\gamma$ -TiAl 合金纳米切削过程的影响, 采用分子动力学数值方法对不同切削晶向下的切削力、切削温度、材料去除及晶格结构变化进行分析和探讨, 揭示不同的晶体取向对单晶  $\gamma$ -TiAl 合金纳米切削质量作用机制。结果表明: 在纳米切削过程中, 随着晶面和晶向的变化, 切削力、切削温度、材料去除和晶格结构都会有不同程度的变化; 选择(010)晶面作为切削平面时切削力较小, 产生的切削热较少,  $\gamma$ -TiAl 合金表面加工质量较好, 晶格结构转变较少; (010)[100]切削晶向下工件产生的切削热较少且最容易切削, 晶格结构转变最少,  $\gamma$ -TiAl 合金表面加工质量最优。

**关键词:** 晶体取向; 纳米切削; 单晶 $\gamma$ -TiAl合金; 材料去除; 分子动力学

---

作者简介: 李俊焯, 男, 1981年生, 博士, 教授, 长春理工大学机电工程学院, 吉林 长春 130022, E-mail: ljj@cust.edu.cn